Mechanism and Prediction of Sound Generation in Reacting Mixing Layers

Toshio MIYAUCHI, Mamoru TANAHASHI and Ye LI
Department of Mechanical and Aerospace Engineering, Tokyo Institute of Technology, 2-12-1 Ookayama, Meguro-ku, Tokyo 152-8552, Japan

Direct numerical simulations have been performed to clarify the sound generation mechanism in two-dimensional chemically reacting mixing layers. The effects of heat release on the mechanism of sound generation are investigated. The pressure fluctuations generated in the reacting mixing layers with heat release are significantly larger than that in the case without heat release, which suggests that the characteristics of sound are mainly determined by the heat release. The acoustic source term in Lighthill's equation is dominated by the entropy component in the case with heat release, while it is governed by the Reynolds stress component in the case without heat release. The far-field sound computed by DNS is compared with the predictions based on the acoustic analogies. In the case with heat release, the acoustic analogies proposed by Lighthill and Powell fail to predict the far-field sound when the source size is selected to be 2Λ. However, the pressure fluctuation in the far field predicted by Lighthill's analogy shows good agreement with the DNS result when the source size is selected to be 3Λ. A new analogy including Powell's acoustic source term and entropy term is proposed, which can predict the far-field sound excellently for both cases of the source size 2Λ and 3Λ.

In addition, DNS has been performed to clarify the mechanism of sound generation in three-dimensional compressible turbulent mixing layers. The amplitude of pressure fluctuation generated in the process of vortex roll-up is relatively low, and it increases significantly with the occurrence of mixing transition. The acoustic source term is relatively small in the process of vortex roll-up, and increases significantly in the period of paring. The magnitude of entropy and Reynolds stress component is nearly the same, which is different from that in the two-dimensional case. The negative Reynolds stress component shows tube-like structure similar to the coherent fine scale eddies, while the entropy component shows sheet-like distribution around coherent fine scale eddies. Lighthill's acoustic analogy can predict far-field sound excellently, while the amplitude of pressure fluctuation predicted by Powell's acoustic analogy shows significantly large values compared with the DNS result.

1. Introduction

In the design process of high efficiency combustor, it is important to reduce the combustion noise and to inhibit the combustion-driven oscillations. Combustion noise is produced by the non-steady oscillation of flame, which is due to the interaction between the vortex structures and flame in the shear flow. Combustion oscillation is caused by enhancement of combustion noise in a combustor by resonance. In order to understand and control these phenomena, it is necessary to make clear the mechanism of sound generation in chemically reacting flows.

The researches on the sound generation can be divided into three groups. The first approach is using acoustic analogy. It includes the Reynolds stress acoustic model proposed by Lighthill (1952), the vortex acoustic model by Powell (1964) and the acoustic model proposed by Möhring (1978). The second approach is experimental one. Laufer et al. (1983) have conducted the experiment on sound generation from low Mach number jet, and investigated the relation between the sound source and the pairing process of large-scale structures in a shear layer. With the recent development of high-speed and large storage computer, analysis of the sound generation by direct numerical simulations (DNS) becomes possible. Ho et al. (1988) have investigated the sound generation in two-dimensional temporally evolving mixing layer. Colonius et al. (1994), Mitchell et al. (1995) have performed the DNS of sound generation by compressible vortex. The far field sound was also predicted using acoustic analogies and compared with the DNS data. Colonius et al. (1997) have also clarified the sound generation in two-dimensional spatially evolving mixing layer.

On the other hand, the recent study (Tanahashi et al. 1997a, 1997b) revealed the existence of coherent fine scale eddies in turbulence. The coherent fine scale eddies show strong swirling motion which is characterized by velocity difference of the order of turbulent intensity ($u'_{\rm rms}$) within the diameter of eight times of kolmogorov microscale (η). These fine scale eddies are expected to bear an important role in the sound generation in turbulence. Especially, in the free shear flows such as mixing layers, the large scale structures are composed of huge number of the coherent fine scale eddies after the mixing transition. However, all the past researches by DNS have been restricted to the two-dimensional flow fields. It is impossible to investigate the effects of coherent fine scale eddies from these results of two-dimensional DNS.

In this study, we first conducted the DNS of two-dimensional chemically reacting compressible mixing layers to clarify the sound generation mechanism. We focus on the determination of principal acoustic source term, the relation between sound generation and chemical reaction and the effects of heat release on the sound generation. Moreover, the far-field sound is predicted by the acoustic analogy. The results predicted by acoustic analogies are compared with the results of DNS. Next, three-dimensional DNS of compressible turbulent mixing layer was performed to investigate the relation between the coherent fine scale eddies and sound generation. In addition, the far-field sound is also predicted using acoustic analogies, and the ability of Lighthill's and Powell's acoustic analogy is evaluated in turbulent mixing layer.

2. Direct numerical simulation of reacting mixing layer

The external forces, Soret effect, Dufour effect, pressure gradient diffusion, bulk viscosity and radiative heat transfer are assumed to be negligible in this work. The chemical reaction is idealized to be a single step, irreversible reaction with heat release (A+B→P+ΔH). The flow field is governed by the mass, momentum, energy and species conservation equations, and the equation of state. The governing equations are non-dimensionalized by the density and temperature of the free-stream flow, the difference of free-stream velocities, and the initial vorticity thickness.

In this study, temporally developing mixing layers are analyzed by DNS. In the case of two-dimensional DNS, periodic boundary condition is used in streamwise (x) direction and non-reflecting boundary condition (NSCBC, Poinsot et al. 1992) is applied in transverse (y) direction. The governing equations are discretized by spectral method in the x direction and by the fourth order central finite difference scheme in the y direction. Aliasing errors from nonlinear terms are fully removed by 3/2 rule in the x direction. A second-order Adams-Bashforth method is used to advance the equations in time. The computational domain in the x and y direction is selected to be 2Λ and 8Λ respectively, where Λ is the most unstable wavelength for the initial mean velocity profile. The simulation is performed on the mesh of 128×1025 for the case of Re=400, Mc=0.2, Pr=0.7, Sc=0.7 and γ=1.4. In order to investigate the effects of heat release, two cases of Ce=1.0, Da=2.0 (with heat release) and Ce=0.0, Da=0.0 (without heat release) are computed. The initial velocity field is composed of a hyperbolic tangent velocity profile and perturbations which contain the most unstable fundamental mode and its subharmonic.

In the case of three-dimensional DNS, periodic boundary conditions are applied in the streamwise (x) and spanwise (z) directions and non-reflecting boundary conditions are used in the transverse (y) direction. The governing equations are discretized by the spectral method in the x and z direction, and by the fourth-order central finite difference scheme in the y direction. A third-order low storage Runge-Kutta scheme is used to advance the governing equations in time. The computational domain in the x, y and z direction is selected to be 2Λ, 6Λ and $4/3\Lambda$ respectively. The simulation is performed on the mesh of 120×1921×80 for the case of Re=600, Mc=0.2, Pr=0.7 and γ=1.4. The initial velocity field is composed of a hyperbolic tangent velocity profile with three-dimensional random perturbations.

3. Mechanism of sound generation in two-dimensional reacting mixing layers

In this section, the DNS results are presented to clarify the mechanism of sound generation in two-dimensional reacting mixing layers. Figure 1 (a) shows the development of momentum thickness defined by

$$\delta_m = \frac{1}{\rho_0 \Delta U^2} \int_{-Ly/2}^{Ly/2} \langle \rho \rangle \left(U_1 - \langle u \rangle \right)\left(\langle u \rangle - U_2 \right) dy \,, \tag{1}$$

where ρ_0 represents the density of free-stream flow, U_1, U_2 and ΔU represent the velocities of high-speed side, low-speed side and the difference of these two respectively. In the mixing layer without heat release, the development of momentum thickness corresponds to the development of large-scale structures. Momentum thickness grows up rapidly in the process of vortex roll-up (t<15), then reaches the plateau, and increases again in the period of pairing (25<t<40). In the case with heat release, the growth rate of momentum thickness is inhibited. The time corresponding to the peak of momentum thickness becomes a little bit earlier due to the effects of heat release.

Figure 1(b) shows the temporal evolution of the pressure fluctuations in the far field. The measurement point is located at 3Λ from the center of shear layer. The time coordinate is shifted to adjust the sound propagating from the center to the measurement point. The pressure fluctuation with relatively low amplitude and high frequency is generated in the process of vortex roll-up, while the amplitude of pressure fluctuation increases significantly in the period of pairing. Moreover, the maximum amplitude of

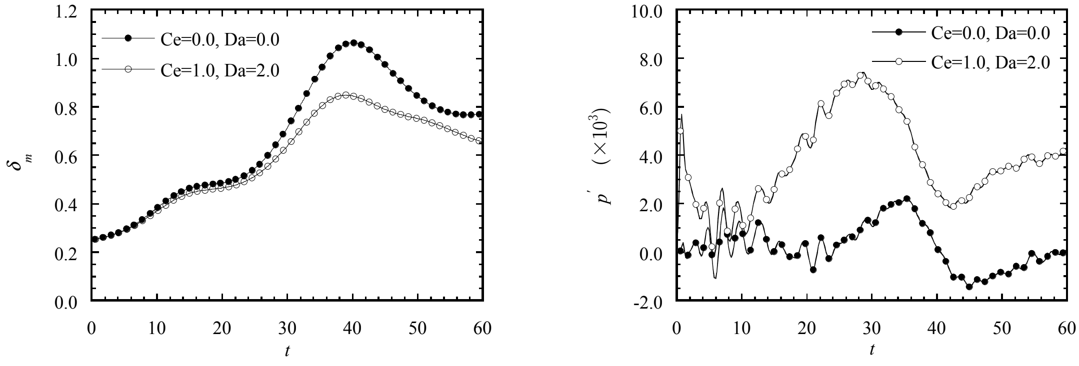

(a) momentum thickness (b) pressure fluctuation

Fig. 1. Temporal evolution of momentum thickness (a) and far-field pressure fluctuations (b).

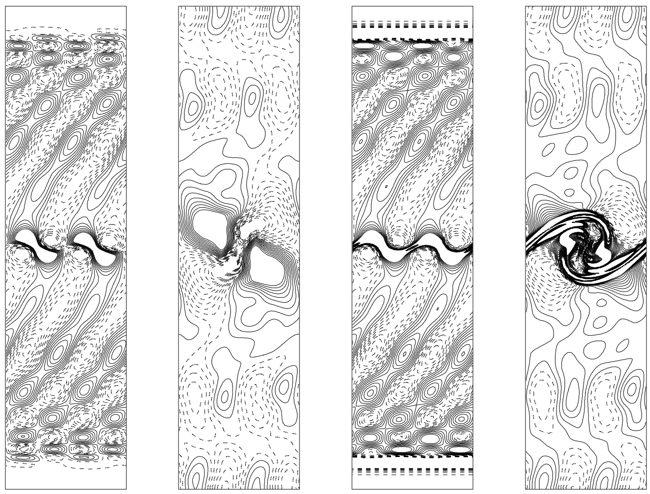

t=10 t=40 t=10 t=40

(a) Ce=0.0, Da=0.0 (b) Ce=1.0, Da=2.0

Fig. 2. Contour plots of dilatation.

pressure fluctuation generated in the mixing layer with heat release is about four times larger than that without heat release. Similar to the variation of momentum thickness, time corresponding to the peak of pressure fluctuation becomes earlier in the case with heat release.

Figure 2 shows the contour plots of dilatation ($d=\nabla\cdot\boldsymbol{u}$) at t=10 and t=40. The solid lines represent the positive values and the dashed lines represent the negative values in these figures. For the case without heat release, the sound source shows quadrupole character in the process of vortex roll-up (t=10), while in the pairing process (t=40) of two large-scale structures, two quadrupole merger to one large quadrupole. For the case with heat release, the heat release rate is relatively low in the early stage of vortex roll-up, and shows weak effects on the sound generation. As a result, the sound source shows quadrupole character similar to that without heat release. However, the sound source can not be approximated by quadrupole in the period of pairing, because the heat release rate increases significantly.

As an acoustic analogy, Lighthill (1952) has rearranged the exact continuity and momentum equations into a wave equation with a source term on the right-hand side as follow:

$$\frac{\partial^2 \rho'}{\partial t^2} - \frac{1}{M^2}\frac{\partial^2 \rho'}{\partial x_i \partial x_i} = \frac{\partial^2 T_{ij}}{\partial x_i \partial x_j}, \tag{2}$$

where T_{ij} is the Lighthill's turbulent stress tensor defined by

$$T_{ij} = \rho u_i u_j + \frac{1}{M^2}\delta_{ij}\left(\frac{1}{\gamma}p - \rho\right) - \frac{1}{Re}\tau_{ij}\,. \tag{3}$$

In this study, the total acoustic source term (T) is decomposed into three parts: Reynolds stress component (T_R), entropy component (T_E) and viscous component (T_V) respectively, which are defined by

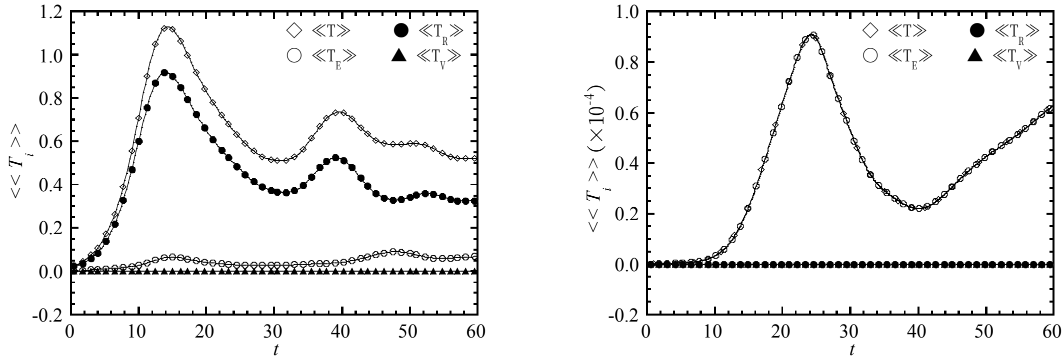

(a) Ce=0.0, Da=0.0 (b) Ce=1.0, Da=2.0

Fig. 3. Contributions of acoustic source terms.

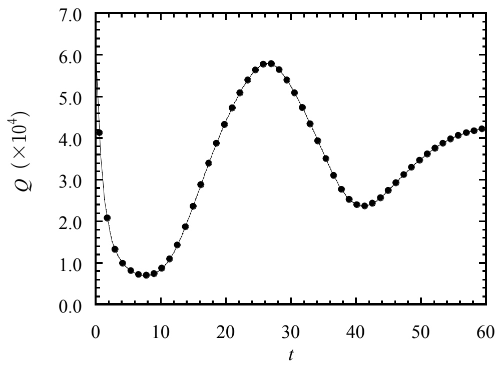

Fig. 4. Temporal evolution of total heat release, Ce=1.0, Da=2.0.

$$T_R = \frac{\partial^2 (\rho u_i u_j)}{\partial x_i \partial x_j}, \tag{4}$$

$$T_E = \frac{\partial^2}{\partial x_i \partial x_j}\left[\frac{1}{M^2}\delta_{ij}\left(\frac{1}{\gamma}p - \rho\right)\right], \tag{5}$$

$$T_V = \frac{\partial^2}{\partial x_i \partial x_j}\left(-\frac{1}{Re}\tau_{ij}\right), \tag{6}$$

$$T = T_R + T_E + T_V . \tag{7}$$

In order to evaluate the magnitude of each acoustic source term, the integration of acoustic source terms defined by

$$<< T_k >>= \int_{-Ly/2}^{Ly/2} \int_0^{Lx} T_k^2 dxdy , \tag{8}$$

is used in this study.

Figure 3 shows the contributions of each acoustic source terms. For the case without heat release, the Reynolds stress component is dominant and shows two peaks at the times corresponding to the vortex roll-up and pairing. However, in the case with heat release, the entropy component is significantly larger than the other two components. The entropy component shows the peak at the time between the vortex roll-up and paring. The viscous component is negligible for these two cases. It can be concluded that the sound generation is governed by the variation of vortex in the case without heat release, while the sound generation is dominated by the chemical reaction in the case with heat release.

Figure 4 shows the development of total heat release rate defined as follow:

$$Q = CeDa \iint \rho^2 Y_A Y_B dxdy . \tag{9}$$

The total heat release rate shows the peak in the period between vortex roll-up and pairing. Temporal evolution of the total heat release rate shows similar profile with the variation of total acoustic source term (Fig. 3(b)). The variation of total heat release rate is also consistent with the pressure fluctuation in the far field (Fig. 1(b)). Accordingly, it is concluded that the sound generation in the reacting mixing layer is determined by the heat release rate.

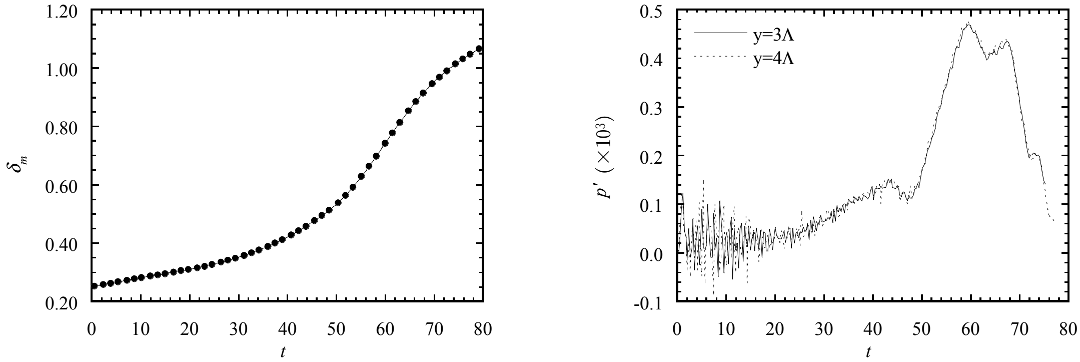

(a) momentum thickness (b) pressure fluctuations

Fig. 5. Temporal evolution of momentum thickness (a) and far-field pressure fluctuations (b).

Here, the relation between entropy component and total heat release rate will be discussed. In the case of perfect gas, if the variations of all quantities are assumed to be small, the continuity and energy conservation equations can be linearised to the following two equations (Lighthill 1978, Tanahashi et al. 1995).

$$\frac{\partial \rho'}{\partial t} = -\rho_0 d \, , \tag{10}$$

$$\frac{\partial p'}{\partial t} = -\gamma p_0 d + q \, , \tag{11}$$

where q represents the total heat release rate. From the above linearised energy equation (Eq. (11)), it can be seen that the variation of pressure fluctuation can be related to the total heat release rate. By using these two equations and the definition of entropy component, the entropy component can be expressed by the following equation.

$$T_E = \frac{\partial^2}{\partial x_i x_j}\left[(p - p_0) - c^2(\rho - \rho_0)\right] = \frac{\partial^2}{\partial x_i x_j}\left(\frac{q}{\rho_0 d}\right). \tag{12}$$

The above equation shows that the entropy component becomes very small in the case without heat release. However, if the chemical reaction release heat, the entropy component is determined by the second spatial derivative of total heat release rate.

4. Mechanism of sound generation in three-dimensional turbulent mixing layers

In this section, the results obtained by three-dimensional DNS are used to clarify the mechanism of sound generation in compressible turbulent mixing layers. Figure 5(a) shows the development of momentum thickness. The growth rate of momentum thickness is nearly constant in the process of vortex roll-up (t<30), while it increases significantly in the period of pairing. The momentum thickness reaches about 4 times the initial value at the final time of DNS.

Figure 5(b) shows the temporal evolution of pressure fluctuations in the far field. The initial pressure fluctuation (t<15) is due to the three dimensional random perturbations of the initial conditions. The pressure fluctuation grows up slowly in the process of vortex roll-up (t<45), while it increases abruptly in the period of paring (50<t<65). In the process of mixing transition (65<t<70), the amplitude of pressure fluctuations show constant value, then decreases significantly after the mixing transition (t>70). It suggests that the mixing transition enhance the amplitude of pressure fluctuation in turbulent mixing layers. Moreover, both the shape and amplitude of the pressure fluctuations are nearly identical (shifted in time by Λ/c_0) at different planes (y=3Λ and 4Λ) in the acoustic far field. This result shows that the sound waves travel with the speed of sound and the spurious numerical dispersion is insignificant.

Figure 6 shows the contributions of each acoustic source term in Lighthill's acoustic analogy. The acoustic source terms show very small values in the process of vortex roll-up and increase significantly in the period of pairing, which is similar to the two-dimensional case (Fig. 3(a)). It has been shown that the entropy component is much smaller than the Reynolds stress component in the case of two-dimensional mixing layer without heat release. However, in the three-dimensional turbulent mixing layer, the magnitude of entropy and Reynolds stress component show nearly the same order. This implies that the mechanism of sound generation in the three-dimensional turbulent mixing layer is different from that in two-dimension. Similar to the two-dimensional case, the viscous component in negligible in the whole period.

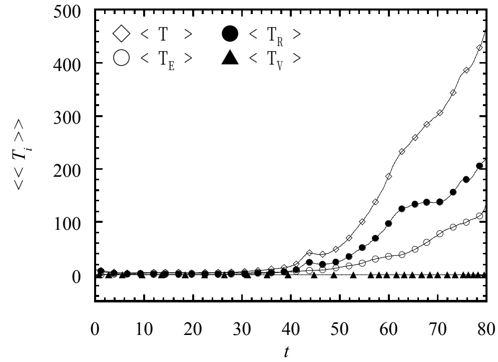

Fig. 6. Contributions of each acoustic source term in Lighthill's acoustic analogy.

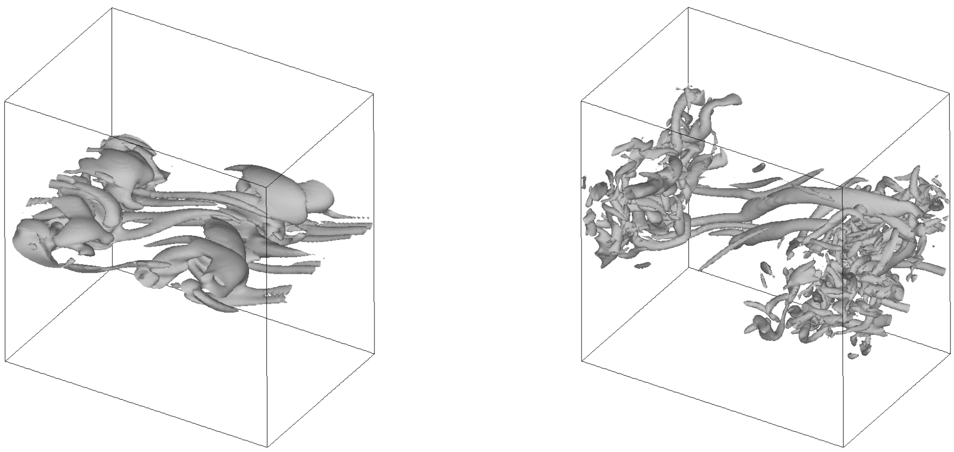

(a) t=40 (Q=0.03) (b) t=80 (Q=0.2)

Fig. 7. Contour surfaces of the second invariant of velocity gradient tensor.

Figure 7 shows the contour surfaces of the second invariant of velocity gradient tensor, which is defined by

$$Q = \frac{1}{2}\left(W_{ij}W_{ij} - S_{ij}S_{ij}\right), \tag{13}$$

where W_{ij} and S_{ij} represent the asymmetric component and symmetric component of velocity gradient tensor. It has been reported by Tanahashi et al. (1997a, 1997b) that the coherent fine scale structure of turbulence is well represented by the positive second invariant region in turbulence. In the process of vortex roll-up (t=40), the streamwise eddies (rib vortices) appear in the braid region, while no fine scale eddy is observed in the core region of large-scale structures. Compared with this, in the period of pairing (t=80), large number of fine scale eddies are observed in the core region. The appearance of these fine scale eddies indicates the occurrence of mixing transition (Tanahashi et al. 1997a).

Figure 8 shows the contour surfaces of Reynolds stress component of acoustic source terms. In the process of vortex roll-up (t=40), although some rib structures appear in the braid region, no fine scale structure is observed in the core region. With the occurrence of mixing transition, Reynolds stress component becomes very complex. After mixing transition (t=80), although the rib structures still exist in the braid region, large number of fine scale structures are observed in the core region. By comparison with contour surfaces of the second invariant (Fig. 9), it can be seen that the structure of Reynolds stress component is identical to the distribution of the second invariant even in the core region where large number of coherent fine scale structures appear. In fact, in the limitation of incompressible flow ($\nabla\cdot\boldsymbol{u}=0$), the relation between Reynolds stress component and the second invariant can be expressed by

$$T_R = -2Q\,. \tag{14}$$

This equation indicates that the mechanism of sound generation and coherent fine scale eddies can be related by means of Reynolds stress component in turbulent mixing layers.

Figure 9 shows the contour surfaces of the entropy component of acoustic source terms. In the process of vortex roll-up (t=40), the entropy component shows sheet-like structure around large-scale spanwise vortices. After the mixing transition (t=80), although the fine scale eddies are formed in the

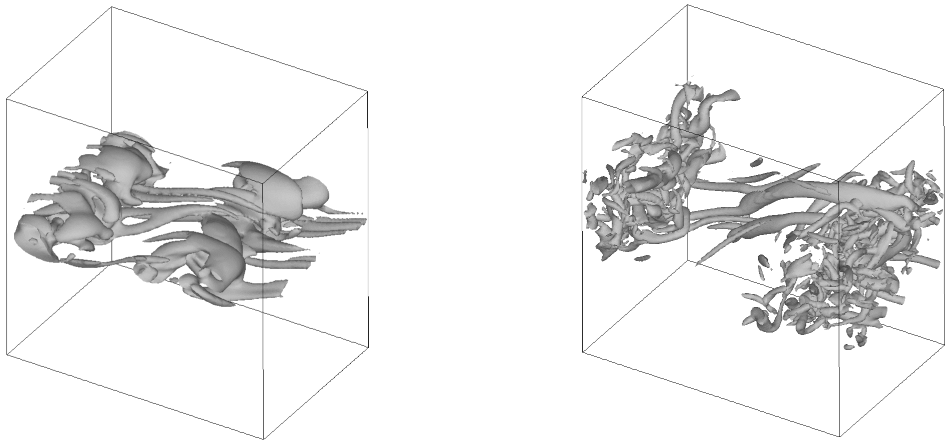

(a) t=40 (T_R=-0.06) (b) t=80 (T_R=-0.4)

Fig. 8. Contour surfaces of Reynolds stress component.

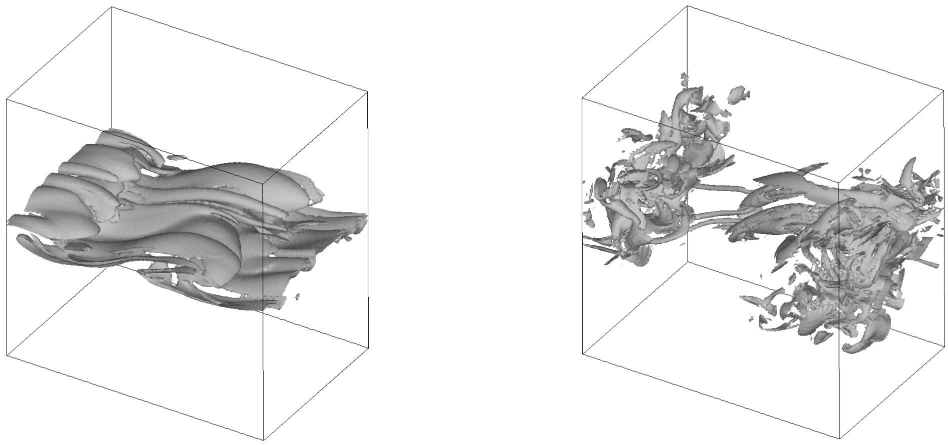

(a) t=40 (T_E=-0.08) (b) t=80 (T_E=-0.6)

Fig. 9. Contour surfaces of entropy component.

core region, the entropy component also shows sheet-like structure around coherent fine scale eddies. It suggests that the coherent fine scale eddies play very important roles in the sound generation in turbulence.

5. Prediction of far-field sound using acoustic analogies

In this section, the pressure fluctuations in the far-field are predicted by using acoustic analogies and compared with the result of DNS. The Lighthill's equation clearly shows that the sound is generated in the turbulent flow. However, it is unclear how the sound is generated from the flow field. In order to clarify this problem, Powell (1964) has proposed a theory of vortex sound and deduced the following wave equation.

$$\frac{\partial^2 \rho'}{\partial t^2} - \frac{1}{M^2}\nabla^2 \rho' = \nabla \cdot (\rho \boldsymbol{\omega} \times \boldsymbol{u}). \tag{15}$$

This equation shows that the variation of vorticity plays an important role in the sound generation. In fact, the relation between Powell's acoustic source terms and Ligthill's acoustic source terms can be expressed as:

$$T = \nabla \cdot \left[\rho \boldsymbol{\omega} \times \boldsymbol{u} + \nabla\left(\tfrac{1}{2}\rho \boldsymbol{u}^2\right) - \tfrac{1}{2}\boldsymbol{u}^2 \nabla \rho + \boldsymbol{u}\nabla \cdot (\rho \boldsymbol{u})\right] + T_E + T_V. \tag{16}$$

It can be seen that the Powell's acoustic source term is a part of the Lighthill's source term.

The wave equations are discretized by the spectral method in the x direction and fourth-order central finite difference scheme in the y direction. A second-order Adams-Bashforth scheme is used to advance the wave equations in time. Periodic boundary condition is applied in the x direction and non-reflecting boundary conditions proposed by Engquist et al. (1979) are used in the y direction. The computational grids are same as those used in the DNS.

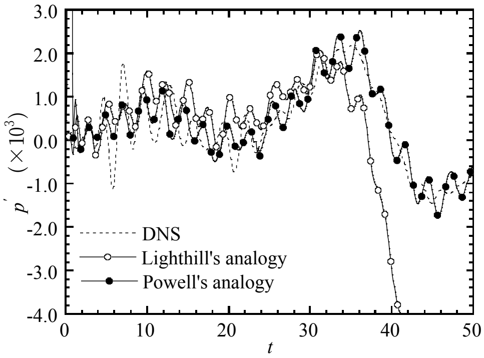

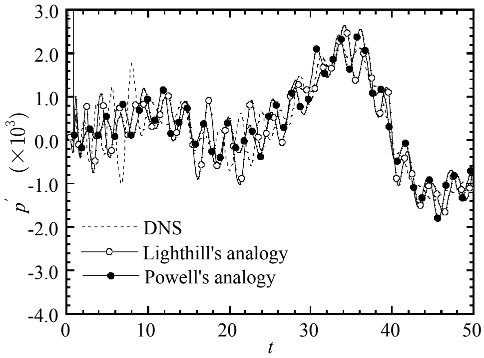

(a) source size: 2Λ (b) source size: 3Λ

Fig. 10. Comparison of pressure fluctuation obtained by DNS and predicted by acoustic analogies, Ce=0.0, Da=0.0.

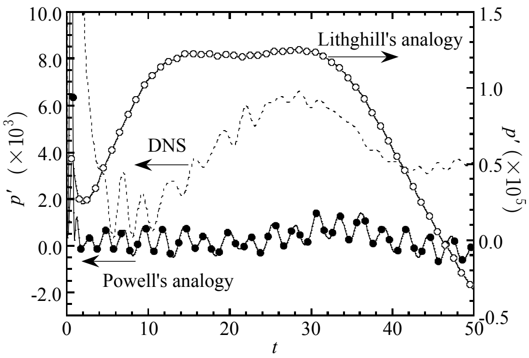

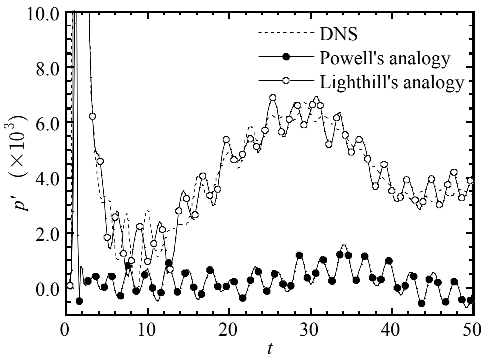

(a) source size: 2Λ (b) source size: 3Λ

Fig. 11. Comparison of pressure fluctuation obtained by DNS and predicted by acoustic analogies, Ce=1.0, Da=2.0.

When the wave equations are used to predict the far-field sound, the size of acoustic source used in the prediction is an important parameter. In the near field, the wave equations with the acoustic source term obtained by the DNS are solved. However, in the far field, the wave equations which express the propagation of sound wave are solved without acoustic source. The source size is defined as the length of near-field in the y direction.

First, we will present the results predicted by acoustic analogies in the case of two-dimensional reacting mixing layers. Figure 10 shows the pressure fluctuations in the far filed predicted by Lighthill's acoustic analogy (Eq. (2)) and Powell's acoustic analogy (Eq. (15)) for the case without heat release. The DNS result is also plotted for comparison. In the case where the source size is selected to be 2Λ, the pressure fluctuations predicted by Lighthill's analogy and Powell's analogy is nearly consistent with the result of DNS in the process of vortex roll-up. In the period of pairing, the pressure fluctuation predicted by Powell's analogy shows good agreement with the DNS result,while the prediction by Lighthill's analogy shows very low level of pressure fluctuation compared with the DNS. However, if the source size is selected to be 3Λ, the pressure fluctuations predicted by Lighthill's acoustic analogy and Powell's acoustic analogy is almost same, which show good agreement with the DNS result. It suggests that 2Λ of source size is enough to represent the Powell's acoustic source, while 3Λ is necessary to represent the Lighthill's acoustic source.

Figure 11 shows the pressure fluctuations in the far filed obtained by DNS and predicted by Lighthill's analogy and Powell's analogy for the case with heat release. The pressure fluctuation predicted by Powell's acoustic analogy is smaller than that of DNS for both cases where the source size is selected to be 2Λ and 3Λ. If the source size is selected to be 2Λ, the pressure fluctuation predicted by Lighthill's acoustic analogy is much larger than that of DNS. However, if the source size is selected to be 3Λ, the pressure fluctuation predicted by Lighthill's acoustic analogy shows good agreement with the DNS result. This suggests that the source size shows very large effect on the pressure fluctuations in the far field when Lighthill's analogy is used to predict the reacting mixing layers.

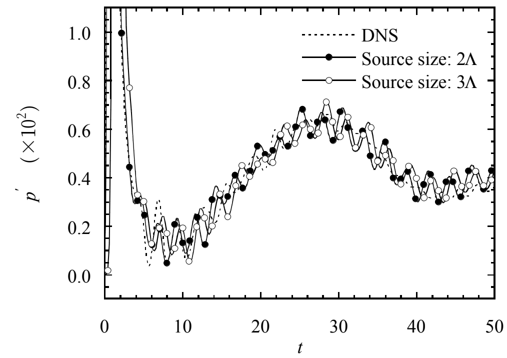

Fig. 12. Comparison of pressure fluctuation obtained by DNS and predicted by proposed acoustic analogy, *Ce*=1.0, *Da*=2.0.

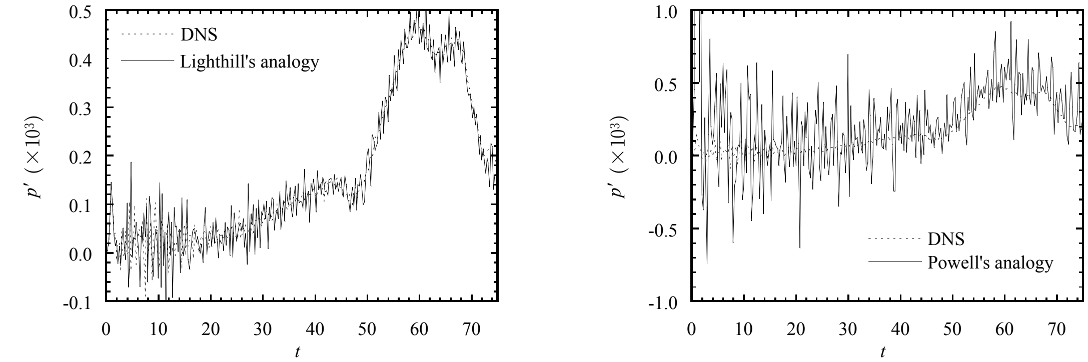

(a) Lighthill's analogy (b) Powell's analogy

Fig. 13. Comparison of pressure fluctuation obtained by DNS and predicted by acoustic analogies. (Three dimensional)

As shown in Fig. 3(b), the entropy component is much larger than the Reynolds stress component in the case with heat release. Therefore, it is expected that the entropy component plays an important role in the sound generation. In this work, we propose the following acoustic analogy equation with the acoustic source terms including Powell's acoustic term and entropy component.

$$\frac{\partial^2 \rho'}{\partial t^2} - \frac{1}{M^2}\nabla^2 \rho' = \nabla \cdot (\rho \boldsymbol{\omega} \times \boldsymbol{u}) + T_E \,. \tag{17}$$

Figure 12 shows the far-field pressure fluctuations predicted by the proposed acoustic analogy. The pressure fluctuations predicted by proposed acoustic analogy show good agreement with the DNS results for the two cases where the source size is selected to be 2Λ and 3Λ respectively. This suggests that the proposed analogy can predict the far-field sound excellently even the small source size is used.

Up to now, we have discussed the prediction of far-field sound using acoustic analogies in the case of two-dimensional reacting mixing layers. Next, the similar result in the three-dimensional case will be presented. Figure 13 shows the far-field pressure fluctuations predicted by Lighthill's and Powell's acoustic analogy in the case of three-dimensional turbulent mixing layers. The DNS result is also plotted for comparison. Here, the source size is selected to be 4Λ. The far–field pressure fluctuation predicted by Lighthill acoustic analogy shows good agreement with the DNS result, although the predicted pressure fluctuation contain some high frequency waves in the whole period. Compared with this, the amplitude of far-field pressure fluctuation predicted by Powell's acoustic analogy shows significantly larger value than the DNS result. It has been shown that Powell's acoustic analogy can predict the far-field sound excellently in the two-dimensional mixing layer. However, Powell's acoustic analogy can not predict far-field sound correctly in the three-dimensional turbulent mixing layer. This result indicates that the mechanism of sound generation in turbulent mixing layer is different from that in two-dimensional case.

6. Conclusions

In this study, first two-dimensional DNS have been carried out to clarify the mechanism of sound generation in the chemically reacting mixing layers and the following conclusions are obtained.

(1) The pressure fluctuations generated in the reacting mixing layer with heat release are significantly larger than that without heat release. The acoustic source term in Lighthill's equation is dominated by entropy component and the Reynolds stress component is considerably small in the case with heat release, while it is governed by the Reynolds stress component in the case without heat release. The viscous component is negligible in both cases.

(2) For the case without heat release, the far-field sound predicted by Lighthill's and Powell's acoustic analogy show good agreement with the DNS result when the source size is selected to be 3Λ. If the source size is selected to be 2Λ, Powell's analogy can predict far-field sound excellently, while the pressure fluctuation predicted by Lighthill's analogy is small compared with the DNS.

(3) For the case with heat release, the far-field sound predicted by Powell's analogy is very small compared with the DNS. The far-field sound by Lighthill's analogy is significantly large compared with the DNS result when the source size is selected to be 2Λ. However, the pressure fluctuation in the far field predicted by Lighthill's analogy shows good agreement with the DNS when the source size is selected to be 3Λ.

(4) A new analogy including Powell's acoustic source term and entropy component is proposed, which can predict the far-field sound excellently for both cases where the source size is selected to be 2Λ and 3Λ.

Next, three-dimensional DNS has also been performed to clarify the mechanism of sound generation in compressible turbulent mixing layers and following conclusions are obtained.

(1) The amplitude of pressure fluctuation generated in the process of vortex roll-up is relatively low, and it increases significantly in the period of pairing. After the mixing transition, the pressure fluctuation decreases abruptly.

(2) The acoustic source term is relatively small in the process of vortex roll-up, and increases significantly in the period of paring. The magnitude of entropy and Reynolds stress component is nearly same, which is different from that in the two-dimensional case. The negative Reynolds stress component shows tube-like structure similar to the coherent fine scale eddies, while the entropy component shows sheet-like distribution around coherent fine scale eddies.

(3) Lighthill's acoustic analogy can predict far-field sound excellently, while the amplitude of pressure fluctuation predicted by Powell's acoustic analogy shows significantly large values compared with the DNS result.

References

Colonius T, Lele S K, Moin P (1994), The scattering of sound waves by a vortex: numerical simulations and analytical solutions. J Fluid Mech 260: 271-298

Colonius T, Lele S K, Moin P (1997), Sound generation in a mixing layer. J Fluid Mech 330: 375-409

Engquist B and Majda A (1979), Radiation boundary conditions for acoustic and elastic wave calculations, Commun Pure Applied Math 23: 313-357

Ho C M, Zohar Y, Moser R D, Roger M M, Lele S K, Buell J C (1988), Phase decorrelation, streamwise vortices and acoustic radiation in mixing layers. Center for Turbulence Research, Proceedings of the Summer Program 1988: 29-39

Laufer J, Yen T C (1983), Noise generation by a low-Mach-number jet. J Fluid Mech 134: 1-31

Lighthill J (1978) Waves in Fluids. Cambridge University Press, 1-5

Lighthill M J (1952), On sound generated aerodynamically I. General theory. Proc R Soc Lond A 211: 564-587

Möhring W (1978), On vortex sound at low Mach number. J Fluid Mech 85 part4: 685-691

Mitchell B E, Lele S K, Moin P (1995), Direct computation of the sound from a compressible co-rotating vortex pair. J Fluid Mech 285: 181-202

Poinsot T J, Lele S K (1992), Boundary conditions for direct simulations of compressible viscous flows. J Comput Phys 101: 104-129

Powell A (1964), Theory of vortex sound. J Acoust Soc Am 36: 177-195

Tanahashi M, Miyauchi T (1995), Interaction between turbulence and chemical reaction in turbulent diffusion flames. Proceeding of the ASME/JSME, Thermal Engineering: 105-110

Tanahashi, M. Miyauchi, T. & Matsuoka, K. (1997a), Coherent fine scale structure in temporally-developing turbulent mixing layer. Turbulence, Heat and Mass Transfer, Vol. 2, 461-470, Delft University Press.

Tanahashi, M. Miyauchi, T. & Ikeda J. (1997b), Scaling law of coherent fine scale structure in homogeneous isotropic turbulence. Turbulence and Shear Flow Phenomena-1, First International Symposium, (eds. Banerjee, S & Eaton, J. K.), 59-64